Journal of Power Sources 195 (2010) 1720–1725

Contents lists available at ScienceDirect

Journal of Power Sources

journal homepage: www.elsevier.com/locate/jpowsour

Short communication

A high performance silicon/carbon composite anode with carbon nanofiber for lithium-ion batteries

Q. Si, K. Hanai, T. Ichikawa, A. Hirano, N. Imanishi, Y. Takeda*, O. Yamamoto

Department of Chemistry, Faculty of Engineering, Mie University, 1577 Kurimamachiya-cho, Tsu, Mie 514-8507, Japan

ARTICLE INFO

Article history:
Received 27 August 2009
Received in revised form
30 September 2009
Accepted 30 September 2009
Available online 9 October 2009

Keywords:
Li-ion batteries
Anode materials
Carbon nanofiber
Si/C composite

ABSTRACT

The electrochemical performance of a composite of nano-Si powder and a pyrolytic carbon of polyvinyl chloride (PVC) with carbon nanofiber (CNF) was examined as an anode for lithium-ion batteries. CNF was incorporated into the composite by two methods; direct mixing of CNF with the nano-Si powder coated with carbon produced by pyrolysis of PVC (referred to as Si/C/CNF-1) and mixing of CNF, nano-Si powder, and PVC with subsequent firing (referred to as Si/C/CNF-2). The external Brunauer–Emmett–Teller (BET) surface area of Si/C/CNF-1 was comparable to that of Si/C/CNF-2. The micropore BET surface area of Si/C/CNF-2 (73.86 $m^2 g^{-1}$) was extremely higher than that of Si/C/CNF-1 (0.74 $m^2 g^{-1}$). The composites prepared by both methods exhibited high capacity and excellent cycling stability for lithium insertion and extraction. A capacity of more than 900 mA h g^{-1} was maintained after 30 cycles. The coulombic efficiency of the first cycle for Si/C/CNF-1 was as low as 53%, compared with 73% for Si/C/CNF-2. Impedance analysis of cells containing these anode materials suggested that the charge transfer resistance for Si/C/CNF-1 was not changed by cycling, but that Si/C/CNF-2 had high charge transfer resistance after cycling. A composite electrode prepared by mixing Si/C/CNF-2 and CNF exhibited a high reversible capacity at high rate, excellent cycling performance, and a high coulombic efficiency during the first lithium insertion and extraction cycles.

1. Introduction

With the development of portable devices such as cellular phones and notebook computers, there is a strong demand for high capacity and high energy density Li-ion batteries. However, the reversible capacity of graphite anodes in Li-ion batteries is only 372 mA h g^{-1} [1], which is approximately one-tenth of the Li anode. Unfortunately, the use of lithium metal as the anode is difficult, due to the formation of dendrites on the lithium anode surface [2]. In recent years, the development of new high-capacity anode materials such as alloys and carbon-based composites has attracted significant interest. It is well known that some elements can electrochemically react with Li to form Li alloy and yield high capacity. Among these elements, Si is most promising, because of its high theoretical capacity (4200 mA h g^{-1} as $Li_{4.4}Si$) and low Li-insertion potential versus Li/Li^+ [3]. However, large volume changes take place during Li-insertion and extraction, which causes pulverization or crumbling of the active materials followed by a loss of electrical contact. As a result, the Si electrode shows a rapid capacity fade [4,5]. Several strategies have been proposed to accommodate the large volume change of Si in order to improve its cyclability. One of the most promising methods is to disperse Si into a carbon matrix [6–8], in which the carbon phase acts as both a structural buffer and an electrochemically active material. Graphite, mesophase microbeads (MCMB), pyrolyzed polyvinyl chloride (PVC), and other carbonaceous materials have been used as matrices for Si [9–14].

Various methods have been employed to prepare Si and carbon composite anodes. Zheng et al. [15] synthesized a nanoporous Si/graphite/carbon composite. The nanoporous Si/graphite composite was prepared via the two-step ball-milling of SiO, Al, and graphite, followed by an etching process with hydrochloric acid. Carbon was then incorporated by the pyrolysis of PVC. The nanoporous Si/graphite/C composite exhibited a reversible capacity of approximately 700 mA h g^{-1} with no capacity loss up to the 120th cycle. However, the first cycle charge-discharge coulombic efficiency was as low as 55%. Liu et al. [11,16] also prepared a silicon/disordered carbon composite by the pyrolysis of PVC, in which high energy mechanical milling (HEMM) was involved between the two thermal pyrolysis processes. The composite offered a large reversible capacity of 1152 mA h g^{-1}; however, the capacity gradually decreased to 66% of the initial capacity after 40 cycles. A relatively high initial cycle coulombic efficiency of approximately 80% was observed. In this study, the electrode materials were cast onto a 300 μm thick Ni foam. Recently, Ji and Zhang [13] reported a high-performance Si and carbon nanofiber composite with a porous structure. The composite was fabricated simply by electrospinning

* Corresponding author. Tel.: +81 59 231 9419; fax: +81 59 231 9489.
E-mail address: takeda@chem.mie-u.ac.jp (Y. Takeda).

0378-7753/$ – see front matter © 2009 Elsevier B.V. All rights reserved.
doi:10.1016/j.jpowsour.2009.09.073

and subsequent carbonization of the mixture of polyacrylonitrile (PAN), poly-L-lactic acid (PLLA) and nano-Si. The resultant porous nano-Si and carbon nanofiber composite anodes exhibited a high initial reversible capacity of 1100 mA h g^{-1}, and a high first cycle coulombic efficiency of 82.1%. However, the reversible capacity retention was not so good. The initial capacity of 1100 mA h g^{-1} was decreased to 600 mA h g^{-1} after 30 cycles. Carbon nanofiber (CNF) was suggested as the negative electrode material [17,18]. CNF features both disordered and graphitic carbon, and this characteristic is expected to overcome the hurdles of lithium batteries for high-power applications, because the CNF anode can deliver high specific capacity even at very high charge-discharge currents, such as a 10 C rate [18–20]. However, the reversible capacity of CNF is not so high and the cyclic performance was poor.

We have previously reported the excellent electrochemical performance of amorphous carbon-coated Si by the pyrolysis of polyvinyl chloride at 900 °C for 2 h [12]. A composite with 52 wt% nano-Si (particle size of 50 nm) and 48 wt% C had an initial discharge capacity of 970 mA h g^{-1} and a low capacity fade by cycling. However, such high performance was obtained for an electrode cast onto a nickel foam and the electrode cast on copper foil also had excellent performance. In this study, we have investigated the high performance carbon-coated nano-Si anode further in order to improve the electrochemical performance of the electrode cast on copper foil, with CNF added to the carbon-coated nano-Si composite for improved contact with the copper substrate and between the electrode materials.

2. Experimental

Nano-Si powder (particle size 50 nm, purity >98%) and PVC were purchased from Aldrich and the CNF (diameter: 10–20 nm, length: 0.1–10 μm) was purchased from Jemco, Japan. The nano-Si and carbon composite (Si/C) was prepared as follows; PVC and nano-Si powder (weigh ratio 9:1) were mixed in tetrahydrofuran (THF) and dried at 60 °C for 5 h. The mixture was then heated at 900 °C for 2 h in 2% H_2–Ar. The product was mixed with CNF (Si/C:CNF weight ratio 60:10) in 1-methyl-2-pyrrolidone (NMP) solution under ultrasonication for 30 min and then stirred for 2 h. The carbon-coated nano-Si and CNF mixed composite is denoted Si/C/CNF-1. A nano-Si, carbon, and CNF composites were also prepared by another route. Nano-Si, CNF and PVC (weight ratio 1:1:9) were mixed in THF under ultrasonication for 30 min, dried at 60 °C for 5 h, and then heated at 900 °C for 2 h in 2% H_2–Ar. The sample obtained by this method is denoted Si/C/CNF-2. A mixed electrode of Si/C/CNF-2 and CNF (weight ratio 75:5) was prepared by the same method as that for Si/C/CNF-1, and was denoted Si/C/CNF-3. On the basis of remaining carbon obtained from heat decomposition of PVC at 900 °C, the Si contents of Si/C, Si/C/CNF-1, Si/C/CNF-2 and Si/C/CNF-3 composites are estimated as about 50%, 43%, 33% and 31%, respectively.

Electrochemical tests of the composite electrodes were conducted using a two-electrode coin-type cell. The working electrodes consisted of the active materials, acetylene black, and poly (vinylidene fluoride) (PVDF) in NMP. The compositions of the electrodes are listed in Table 1. The mixtures of the electrode components in NMP were cast onto copper foils, and dried at 80 °C for 1 h. The cast electrodes were cut to a size of 1 cm × 1 cm. The weights of active material in the electrodes were in the range of 0.2–1 mg. The electrode was further dried at 120 °C under vacuum for 1 h, followed by pressing at 200 kg f cm^{-2}. Coin-cells (type 2025) were assembled in an Ar-filled glove box using 1 M $LiClO_4$ in an ethylene carbonate (EC) and diethylene carbonate (DEC) mixed solution (1:1 in volume) as the electrolyte and metallic lithium foil (20 μm in thickness) as the counter electrode. The electrochemical performance of the composite anode was evaluated using constant current charge-discharge cycling in the voltage range of 20–1500 mV at room temperature. The specific capacity was based on the weight of Si/C for the Si/C and Si/C/CNF-1 electrodes and that of Si/C/CNF for the Si/C/CNF-2 and Si/C/CNF-3 electrodes.

Table 1
Compositions of composite electrodes (in wt%).

Electrode	Si/C	Si/C/CNF	CNF	AB	PVDF
Si/C	60%	–	–	20%	20%
Si/C/CNF-1	60%	–	10%	10%	20%
Si/C/CNF-2	–	60%	–	20%	20%
Si/C/CNF-3	–	75%	5%	–	20%

Table 2
BET surface areas of the Si/C, Si/C/CNF-1, and Si/C/CNF-2 electrode materials.

Material	Total surface area (m^2 g^{-1})	Micropore surface area (m^2 g^{-1})	External surface area (m^2 g^{-1})
Si/C	29.47	13.59	15.88
Si/C/CNF-1	37.32	0.74	36.59
Si/C/CNF-2	107.05	73.86	33.19

X-ray diffraction (XRD) patterns were obtained using a Rigaku Rotaflex RU-200B diffractometer with Cu Kα radiation. The morphology of the composite electrode was examined using scanning electron microscopy (SEM; Hitachi SEM S-4000) and transmission electron microscopy (TEM; JEOL JEM-1011). The impedance measurement was performed using an impedance/gain-phase analyzer (Solartron SI1260) and an electrochemical interface (Solartron SI1287), using a beaker cell with a lithium metal reference electrode. Surface area and porosity measurements were carried out using a gas absorption analyzer (Shimadzu Micromeritics TriStar 3000).

3. Results and discussion

The surface areas of the composite electrodes measured using the Brunauer–Emmett–Teller (BET) method are shown in Table 2. The surface area of Si/C/CNF-1 is slightly larger than that of Si/C. However, the micropore surface area is drastically reduced by mixing CNF in Si/C. The micropores in Si/C were diminished during the mixing process, but the mechanism for this is not clear. Fig. 1 shows TEM images of CNF, Si/C, and Si/C/CNF-1. The as-received CNF has a uniform size distribution with a diameter of approximately 20 nm, as shown in Fig. 1a. After ultrasonic mixing with CNF in NMP (see Fig. 1c), the Si/C is uniformly dispersed into the CNF matrix.

Fig. 2 compares the voltage profiles and cycling stability of the Si/C and Si/C/CNF-1 electrodes for lithium insertion and extraction at room temperature. Both electrodes exhibited a sloping potential plateau between 1.1 and 0.1 V in the first lithium insertion process. Si/C/CNF-1 electrode suffered a larger irreversible capacity. The reason can be attributed to the formation of a solid electrolyte interface (SEI) layer, and the trapping of Li ions in the "cuplike" cavity of the bamboo shaped CNF [18]. Li insertion into silicon occurs at potentials below 0.1 V, yielding an extremely large capacity. The coulombic efficiency of Si/C/CNF-1 for the first cycle is 53%, which is lower than that of the bare Si/C composite (74%). This is due to the extremely large irreversible capacity that CNF itself exhibits during the first lithium insertion process, as shown in the inset in Fig. 2a. After the second cycle, the lithium insertion and extraction efficiency was almost 100%. Fig. 2b shows the cycling stability of the Si/C and Si/C/CNF-1 electrodes. Note that although the Si/C electrode shows a higher second cycle lithium insertion capacity of ca. 1204 mA h g^{-1}, it rapidly drops to 557 mA h g^{-1} after 30 cycles with a retention rate of only 46%. For the Si/C/CNF-1 electrode, the second cycle capacity of 1000 mA h g^{-1} is lower than that of the Si/C electrode, but the retention rate after 30 cycles is as high as

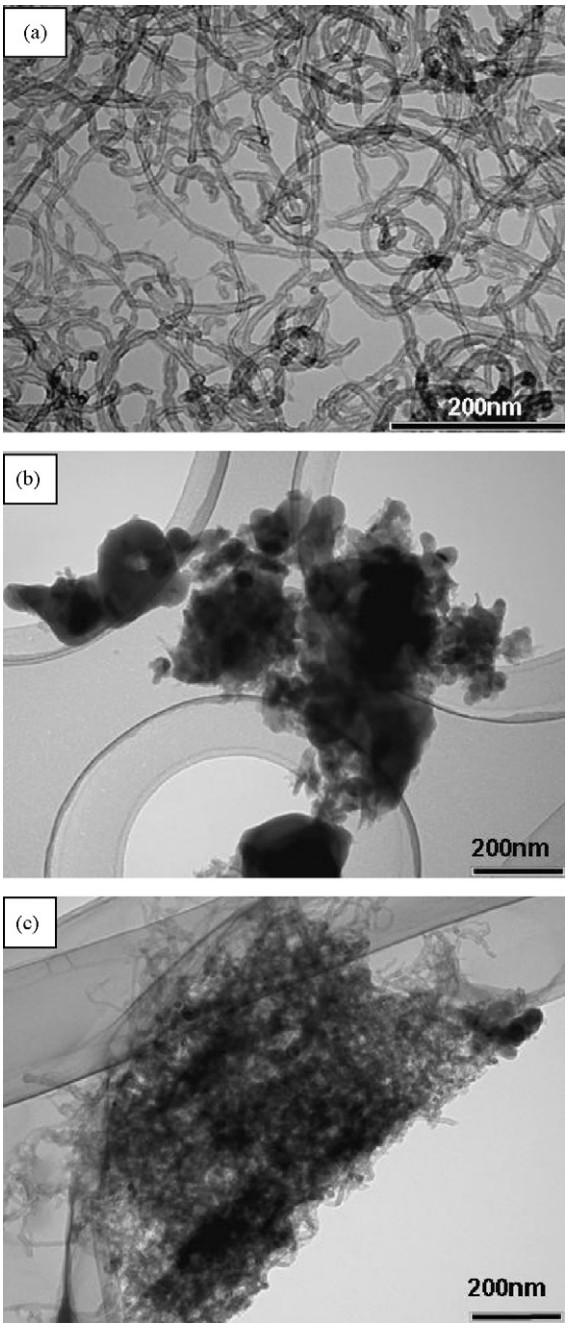

Fig. 1. TEM images of (a) CNF, (b) Si/C, and (c) Si/C/CNF-1.

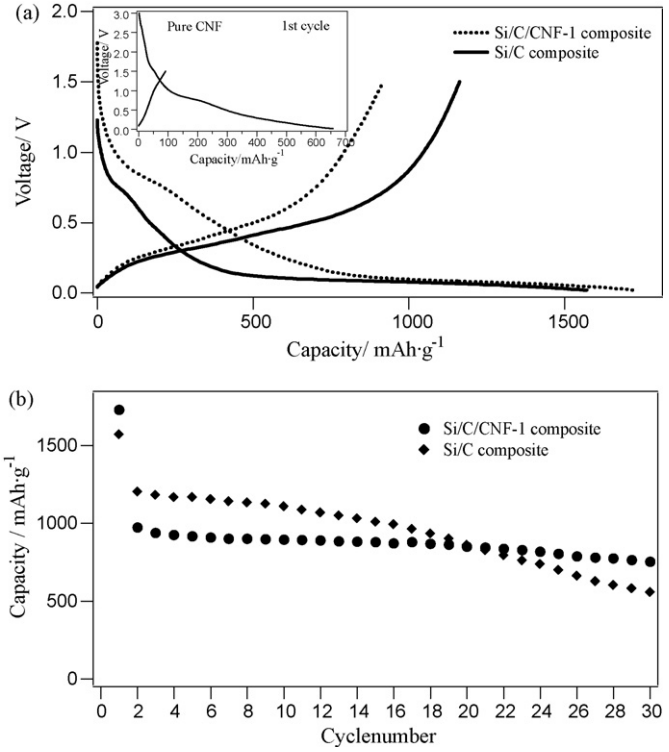

Fig. 2. (a) Voltage vs. lithium insertion capacity curves and (b) cycling performance for Si/C and Si/C/CNF-1 at room temperature. Current rate 1/10 C; cut-off voltage 20–1500 mV.

77%. Ji and Zhang [13] reported that the CNF and nano-Si composite electrode exhibits a high initial lithium insertion capacity of 1100 mA h g^{-1} and a high coulombic efficiency at the first cycle of 82%. However, the retention rate of the lithium insertion capacity was only 57% after 30 cycles. As Si/C/CNF-1 was prepared by the direct mixing of CNF and Si/C, CNF may float mainly on the surface of the Si/C particles, and as a result, CNF may contact directly with the electrolyte, resulting in large initial irreversible capacity from CNF.

The Si/C/CNF-2 composite was also prepared through the other route, where CNF was covered with pyrolytic carbon derived from PVC. CNF, nano-Si and PVC were mixed and then heated, so that nano-Si and CNF were covered with the PVC-derived pyrolytic carbon. Fig. 3 shows an XRD pattern of Si/C/CNF-2 with diffractions of silicon and carbon, but absent of silicon oxide and C–Si alloy diffractions. The broad peak at approximately 25.3° can be attributed to CNF. Fig. 4 shows a TEM image of nano-Si, a mixture of nano-Si and CNF, and Si/C/CNF-2. The nano-Si powders are well dispersed in the CNF matrix by ultrasonic mixing in THF, as shown in Fig. 4b. Note that Si/C/CNF-2 has a porous structure (Fig. 4c). The BET surface area of Si/C/CNF-2 is 107.1 m^2 g^{-1}, which is significantly higher than that of Si/C/CNF-1. Such a structure offers more free space to buffer the volume changes of Li_xSi during the Li insertion and extraction process [13]. Fig. 5a compares the voltage versus lithium insertion specific capacity curves for Si/C/CNF-1 and Si/C/CNF-2. Note that Si/C/CNF-2 shows a higher coulombic efficiency of 71%, compared with that of Si/C/CNF-1 (53%). This is due to the covering of the CNF surfaces in Si/C/CNF-2 with the pyrolytic carbon derived from PVC, so that CNF does not directly contact the electrolyte solution. The lithium insertion and extraction cyclic performance of Si/C/CNF-2 is comparable to that of Si/C/CNF-1, as shown in Fig. 5b. The capacity retention is as high as 78% after 30 cycles.

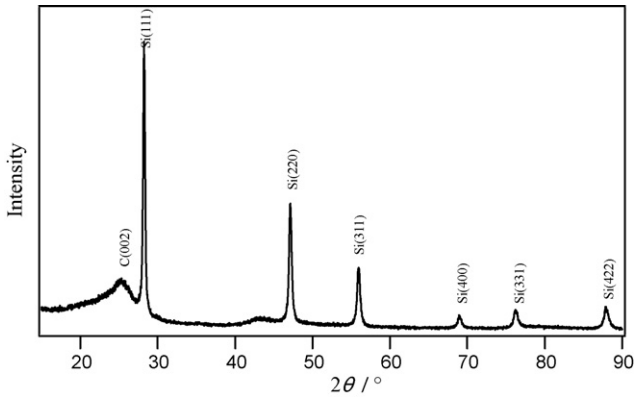

Fig. 3. XRD pattern of Si/C/CNF-2.

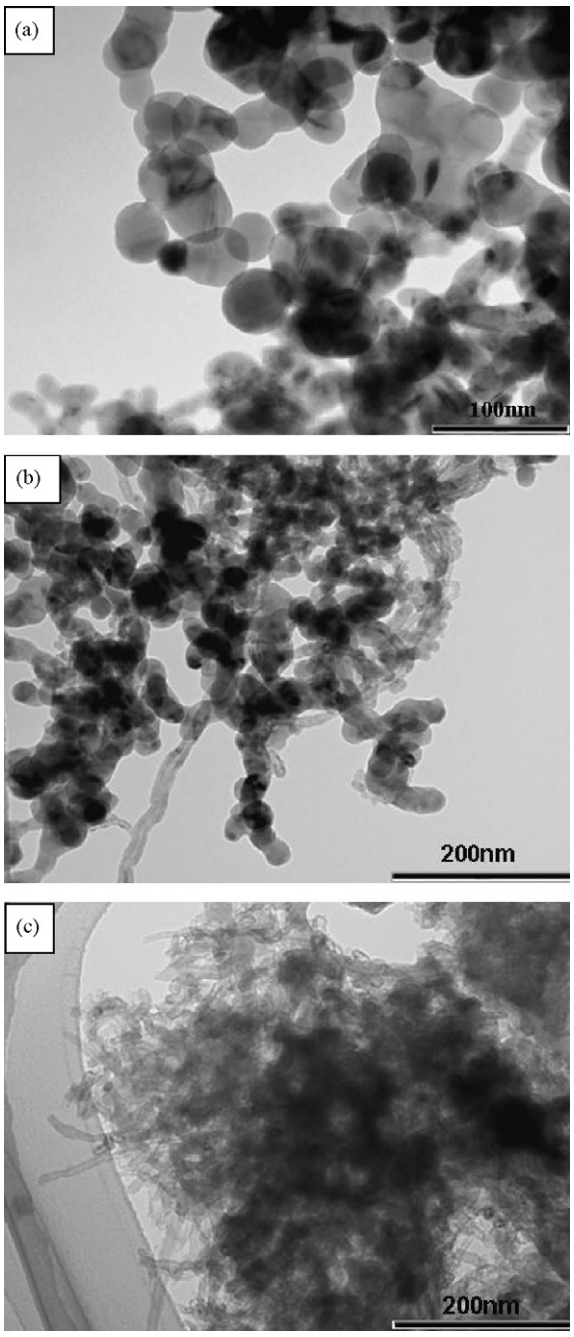

Fig. 4. TEM images of (a) nano-Si powder, (b) Si/CNF mixture, and (c) Si/C/CNF-2.

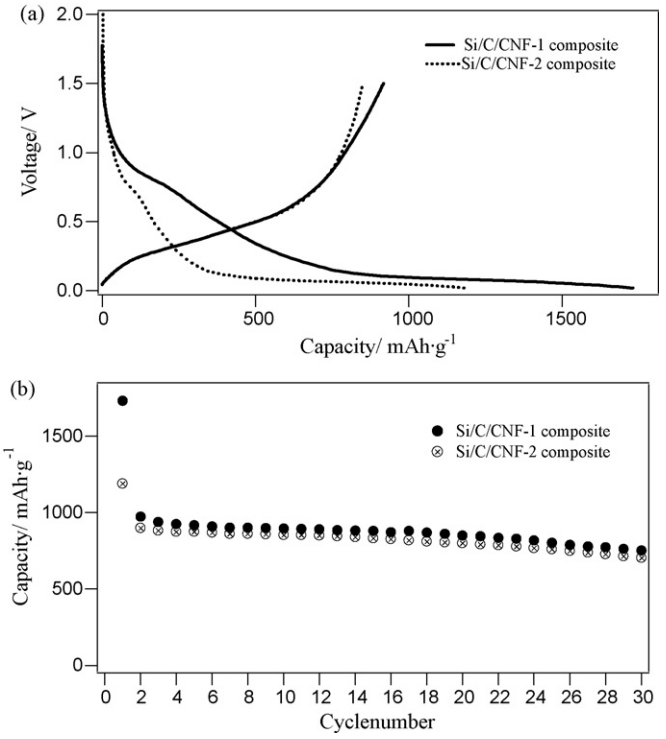

Fig. 5. (a) Voltage vs. lithium insertion capacity curves and (b) cycling performance for Si/C/CNF-1 and Si/C/CNF-2 at room temperature. Current rate 1/10 C; cut-off voltage 20–1500 mV.

The improved electrochemical performance of the Si/C/CNF-1 and Si/C/CNF-2 composites compared with bare Si/C could be ascribed to the buffering effect of the nanosize CNF matrix, which accommodates the large Si volume expansion and shrinkage during lithium insertion and extraction, which ensures good electronic contact between Si and carbon, imparts many active sites for charge transfer reactions, and preserves the integrity of the electrode structure [13].

It is important to observe the microstructural changes before and after the cycling tests. Fig. 6 shows SEM images of Si/C/CNF-1 and Si/C/CNF-2 before and after 50 cycles. Fig. 6b shows that the composite Si/C/CNF-1 electrode keeps the homogeneous surface morphology and shows no obvious cracks even after 50 electrochemical cycles. From Fig. 6c and d, we can see that the porous structure of the Si/C/CNF-2 electrode still remains after cycling. However, the exfoliation of Si/C/CNF-2 from the copper substrate was observed after 20 cycles when a breaker cell was used for measuring the impedance. The impedance profiles of Si/C/CNF-1 and Si/C/CNF-2 before cycling and after 20 cycles are shown in Fig. 7. The impedance profiles show a semicircle in the high frequency range and a diminished semicircle in the low frequency range. The high frequency semicircle could be attributed to the formation of an SEI caused by the decomposition of the electrolyte solution, and the low frequency semicircle to the charge transfer resistance [7]. Si/C/CNF-1 shows a higher interface resistance from the SEI, which is confirmed by the high irreversible capacity at the first lithium insertion and extraction cycle. No significant change of the impedance profile before and after cycling is observed for Si/C/CNF-1. On the other hand, Si/C/CNF-2 shows a relatively low SEI resistance and a significant increase in the second semicircle by cycling, that is, an increase of the charge transfer resistance by cycling. These results indicate that the active site area for the charge transfer decreases with lithium insertion and extraction cycling. The decrease of in active site area may be due to reduced triple phase boundary between the electrode active material, current collector, and the electrolyte.

Si/C/CNF-1 showed a high reversible capacity and excellent cycling performance, but a high irreversible capacity was observed at the first lithium insertion and extraction cycle. However, Si/C/CNF-2 exhibited a high reversible capacity and a low irreversible capacity at the first lithium insertion and extraction cycle, but the charge transfer resistance was increased by lithium insertion and extraction cycling. To overcome these weak points of Si/C/CNF-1 and Si/C/CNF-2, a composite electrode of Si/C/CNF-2 and CNF (Si/C/CNF-3) was prepared. Fig. 8 shows a TEM image of Si/C/CNF-3. There is a homogeneous distribution of Si/C/CNF-2 in the CNF matrix. The voltage versus lithium insertion capacity curve and the cyclic performance are shown in Fig. 9 along with that for Si/C/CNF-2, where the lithium insertion and extraction rate was as high as 1/2 C for Si/C/CNF-3 and 1/10 C for Si/C/CNF-

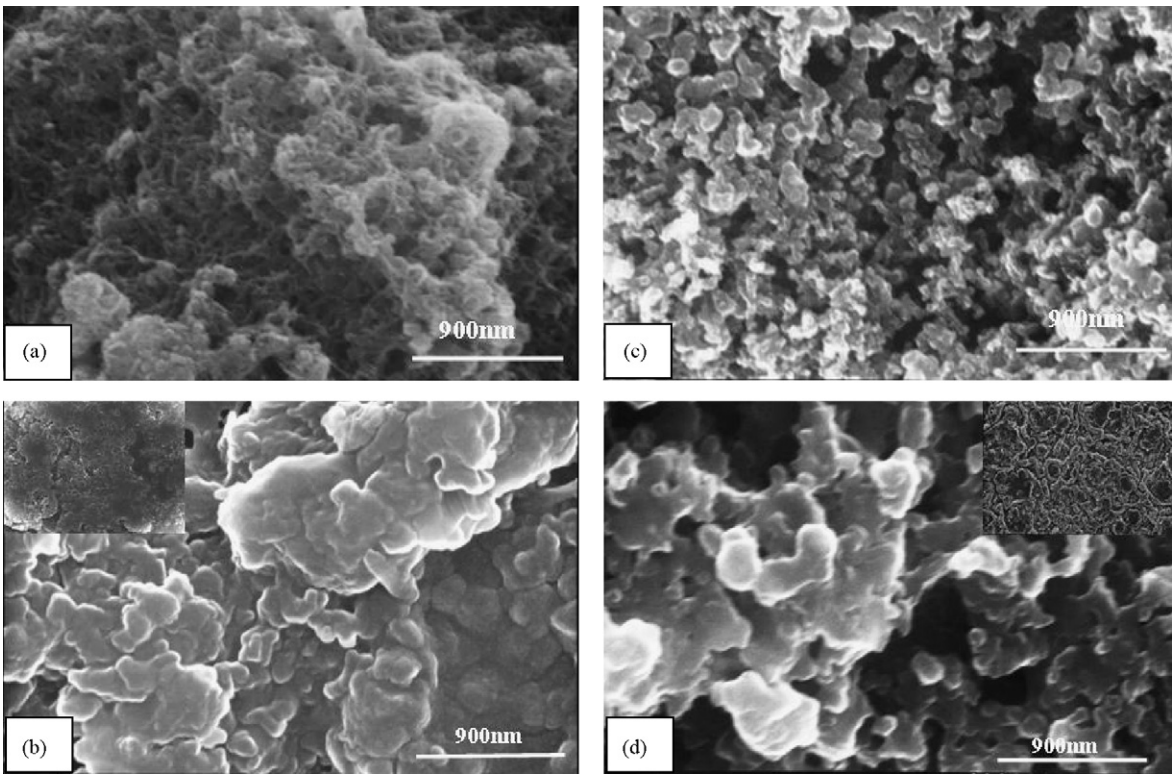

Fig. 6. SEM images of (a) Si/C/CNF-1 before cycling test, (b) Si/C/CNF-1 after 50th lithium insertion and extraction cycle test, (c) Si/C/CNF-2 before cycling test, and (d) Si/C/CNF-2 after 50th lithium insertion and extraction cycle test.

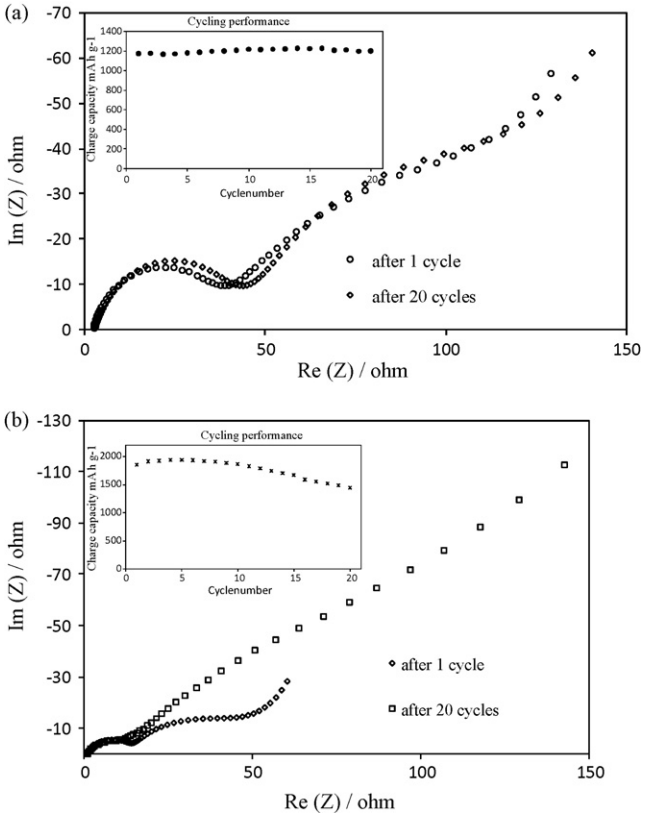

Fig. 7. Impedance profiles for (a) Si/C/CNF-1 and (b) Si/C/CNF-2 after the first and 20th lithium insertion and extraction cycle tests.

2. Although Si/C/CNF-3 shows a slightly lower retention rate of 72% compared with 76% for Si/C/CNF-2 after 30 cycles, it exhibits a higher discharge capacity even at a high rate of 1/2 C, compared with that of Si/C/CNF-2 at a 1/10 C rate. After 30 lithium insertion and extraction cycles, Si/C/CNF-3 still maintains a capacity of 931 mA h g^{-1}. Fig. 10 shows the impedance profile change for the Si/C/CNF-3 electrode after the first and 20th lithium insertion and extraction cycle tests. It is quite interesting that the charge transfer resistance of the Si/C/CNF-3 electrode becomes very low by lithium insertion and extraction cycling. The improvement in the electrochemical performance could be attributed to good electrical contact between the active materials, CNF, and the current collector during the lithium insertion and extraction cycles. This result supports the high rate performance of CNF reported by Subramanian et al. [18].

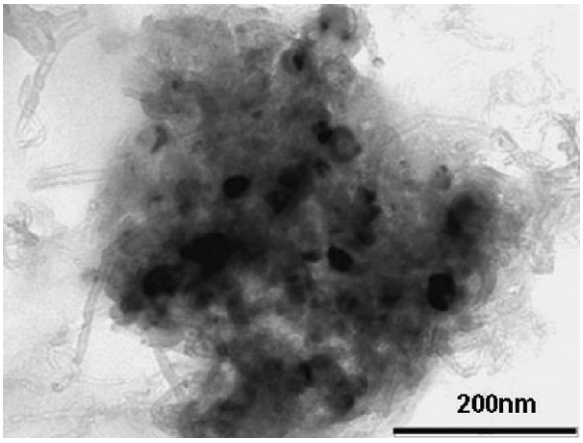

Fig. 8. TEM image of Si/C/CNF-3.

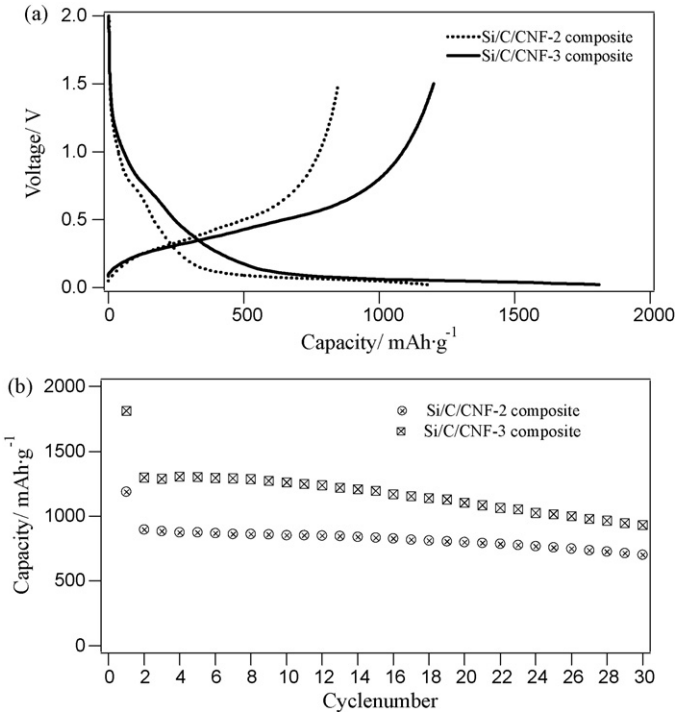

Fig. 9. (a) Voltage vs. lithium insertion capacity curves and (b) cycling performance for Si/C/CNF-2 and Si/C/CNF-3 at room temperature. Current rate 1/10 C for Si/C/CNF-2 and 1/2 C for Si/C/CNF-3; cut-off voltage 20–1500 mV.

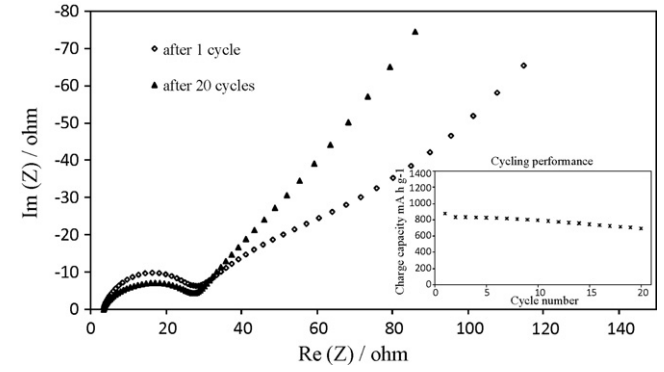

Fig. 10. Impedance profiles for Si/C/CNF-3 after the first and 20th lithium insertion and extraction cycle tests.

4. Conclusions

The lithium insertion and extraction performance of nano-Si, carbon, and carbon nanofiber composite electrodes as lithium electrodes was examined. The composite electrode prepared by mixing carbon-coated nano-Si powder and CNF (Si/C/CNF-1) showed a high reversible capacity and excellent cycling performance, but the first cycle irreversible capacity was high. The composite electrode prepared by heating a mixture of nano-Si, CNF, and PVC (Si/C/CNF-2) showed a high reversible capacity, excellent cyclic performance and low irreversible capacity at the first lithium insertion and extraction cycle. However, a high charge transfer resistance was observed after further lithium insertion and extraction cycles. The best electrode performance was obtained for the composite electrode prepared by mixing Si/C/CNF-2 and CNF. A reversible capacity of 1000 mA h g^{-1} was observed at a high current rate of 1/2 C after 30 lithium insertion and extraction cycles, and a lower irreversible capacity was obtained in the first cycle than that of the Si/C/CNF-1 electrode. High reversible capacity and fairly good cyclability result from utilizing the ductile CNF matrix to buffer the Si volume expansion on the macro domain and maintain good contact with both the active materials and the electrolyte after lithium insertion and extraction cycles.

Acknowledgement

This work was supported by the Cooperation of Innovative Technology and Advanced Research in Evolution Area (City Area) Project of the Ministry of Education, Culture, Sports, Science and Technology of Japan.

References

[1] S. Hossain, Y.-K. Kim, Y. Saleh, R. Loutfy, J. Power Sources 114 (2003) 264.
[2] J. Yamaki, in: M. Wakihara, O. Yamamoto (Eds.), Lithium Ion Batteries, Kodansha, Wiley-VCH, Tokyo, 1998, p. 67.
[3] C.K. Chan, H. Peng, G. Liu, K. McIlwrath, X.F. Zhang, R.A. Huggins, Y. Cui, Nat. Nanotechnol. 3 (2008) 31.
[4] C.K. Chan, R. Ruffo, S.S. Hong, R.A. Huggins, Y. Cui, J. Power Sources 189 (2009) 34.
[5] B.C. Kim, H. Ueno, T. Satou, T. Fuse, T. Ishihara, M. Ue, M. Senna, J. Electrochem. Soc. 152 (2005) A523.
[6] Z.J. Luo, D.D. Fan, X.L. Liu, H.Y. Mao, C.F. Yao, Z.Y. Deng, J. Power Sources 189 (2009) 16.
[7] P.J. Zuo, G.P. Yin, Y.L. Ma, Electrochim. Acta 52 (2007) 4878.
[8] P.J. Zuo, G.P. Yin, Z.L. Yang, Z.B. Wang, X.Q. Cheng, D.C. Jia, C.Y. Du, Mater. Chem. Phys. 115 (2009) 757.
[9] P.J. Zuo, Z.B. Wang, G.P. Yin, D.C. Jia, X.Q. Cheng, C.Y. Du, P.F. Shi, J. Mater. Sci. 43 (2008) 3149.
[10] J. Xie, G.S. Cao, X.B. Zhao, Mater. Chem. Phys. 88 (2004) 295.
[11] Y. Liu, K. Hanai, J. Yang, N. Imanishi, A. Hirano, Y. Takeda, Solid State Ionics 168 (2004) 61.
[12] Q. Si, K. Hanai, N. Imanishi, M. Kubo, A. Hirano, Y. Takeda, O. Yamamoto, J. Power Sources 189 (2009) 761.
[13] L.W. Ji, X.W. Zhang, Electrochem. Commun. 11 (2009) 1146.
[14] Y. Liu, Z.Y. Wen, X.Y. Wang, A. Hirano, N. Imanishi, Y. Takeda, J. Power Sources 189 (2009) 733.
[15] Y. Zheng, J. Yang, J.L. Wang, Y.N. NuLi, Electrochim. Acta 52 (2007) 5863.
[16] Y. Liu, K. Hanai, J. Yang, N. Imanishi, A. Hirano, Y. Takeda, Electrochem. Solid-State Lett. 7 (2004) A369.
[17] H. Habazaki, M. Kiriu, H. Konno, Electrochem. Commun. 8 (2006) 1275.
[18] V. Subramanian, H.W. Zhu, B.Q. Wei, J. Phys. Chem. B 110 (2006) 7178.
[19] L.W. Ji, X.W. Zhang, Electrochem. Commun. 11 (2009) 684.
[20] L.W. Ji, X.W. Zhang, Electrochem. Commun. 11 (2009) 795.